JCTC Journal of Chemical Theory and Computation

Article

pubs.acs.org/JCTC

Perturbation Approach for Computing Infrared Spectra of the Local Mode of Probe Molecules

Rui-Jie Xue,[†] Adam Grofe,[‡] He Yin,[†] Zexing Qu,[†] Jiali Gao,*[,†,‡] and Hui Li*[,†]

[†]Institute of Theoretical Chemistry, Jilin University, 2519 Jiefang Road, Changchun 130023, People's Republic of China

[‡]Department of Chemistry and Supercomputing Institute, University of Minnesota, 207 Pleasant Street, SE, Minneapolis, Minnesota 55455, United States

Supporting Information

ABSTRACT: Linear and two-dimensional infrared (IR) spectroscopy of site-specific probe molecules provides an opportunity to gain a molecular-level understanding of the local hydrogen-bonding network, conformational dynamics, and long-range electrostatic interactions in condensed-phase and biological systems. A challenge in computation is to determine the time-dependent vibrational frequencies that incorporate explicitly both nuclear quantum effects of vibrational motions and an electronic structural representation of the potential energy surface. In this paper, a nuclear quantum vibrational perturbation (QVP) method is described for efficiently determining the instantaneous vibrational frequency of a chromophore in molecular dynamics simulations. Computational efficiency is achieved through the use of (a) discrete variable representation of the vibrational wave functions, (b) a perturbation theory to evaluate the vibrational energy shifts due to solvent dynamic fluctuations, and (c) a combined QM/MM potential for the systems. It was found that first-order perturbation is sufficiently accurate, enabling time-dependent vibrational frequencies to be obtained on the fly in molecular dynamics. The QVP method is illustrated in the mode-specific linear and 2D-IR spectra of the H−Cl stretching frequency in the HCl−water clusters and the carbonyl stretching vibration of acetone in aqueous solution. To further reduce computational cost, a hybrid strategy was proposed, and it was found that the computed vibrational spectral peak position and line shape are in agreement with experimental results. In addition, it was found that anharmonicity is significant in the H−Cl stretching mode, and hydrogen-bonding interactions further enhance anharmonic effects. The present QVP method complements other computational approaches, including path integral-based molecular dynamics, and represents a major improvement over the electrostatics-based spectroscopic mapping procedures.

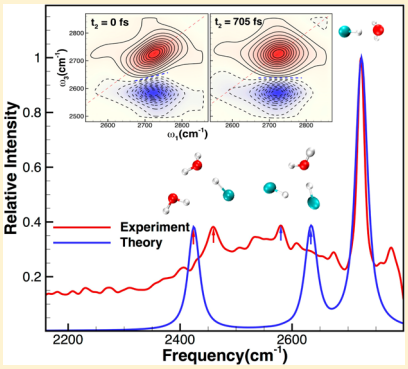

1. INTRODUCTION

Molecular vibrations and infrared spectroscopy of small chromophore probes embedded in molecular clusters, solutions, and biomacromolecules have been widely used to investigate solute−solvent interactions, hydrogen-bonding dynamics, and the local electric fields in enzymes.[1−9] Vibrational frequency shifts are especially sensitive to the local electrostatic environment, which can be easily and accurately measured. Thus, the study of vibrational frequency shifts is an efficient way to analyze the local structure and its consequent electric field.[2,10] Furthermore, measurements of the time-dependent frequency fluctuations or spectral diffusion can provide dynamic information, and it is useful to carry out condensed-phase simulations of solutions or biomacromolecules. To this end, a range of computational methods have been developed for the study of molecular vibration in condensed phases, including path integral simulations.[4,11,12] Still, it is a challenging task to determine the instantaneous vibrational frequencies of probe molecules that include nuclear quantum effects on the fly in molecular dynamics simulations.[1,4,13] In this study, we present a combined quantum mechanical and molecular mechanical (QM/MM) perturbation approach to efficiently and accurately determine the vibrational frequency of a probe molecule to construct its linear and two-dimensional infrared (2D-IR) spectra.[14,15]

We use the HCl−water cluster system to illustrate and validate the present first-order quantum vibration perturbation (QVP1) approach because strong hydrogen-bonding and dispersion interactions are important and because it has been extensively investigated experimentally[16−27] and theoretically.[25−53] Although this appears to be a small test case, it is in fact challenging because of the strong bond-dissociation character in the oscillator mode. We emphasize that the QVP1 method is equally efficient for condensed-phase simulations as in a combined QM/MM approach.[54] This is illustrated on the vibrational spectral shifts of the carbonyl stretch mode of acetone in aqueous solution. The C═O stretch vibration is widely used as a probe to the secondary structure of proteins.[55−58]

Experimentally, Suhm and co-workers reported the first IR spectrum of HCl−water clusters[16,17] and found that a

Received: July 23, 2016
Published: November 22, 2016

DOI: 10.1021/acs.jctc.6b00733
J. Chem. Theory Comput. 2017, 13, 191−201

minimum of four water molecules is required for HCl dissociation. Recently, Havenith and co-workers confirmed that the broad band at 2675 cm^{-1} is due to the dissociated cluster, $H_3O^+(H_2O)_3Cl^-$.[59] On the theoretical side, Born–Oppenheimer molecular dynamics (BOMD) simulations with DFT-based potentials have been used to mode $HCl(H_2O)_n$ (n = 1–4) clusters.[38,40−45,47,60] Marx and co-workers[47] obtained the IR spectra of the HCl–water clusters using the BLYP density functional. A sequential solvation process was proposed to account for the HCl dissociation mechanism, involving the interplay of quantum tunneling and thermal fluctuations from path integral simulations.[33,37,43−45] Employing a semiempirical PM3-MAIS potential, Lin and Paesani extended the investigation to larger clusters up to n = 21.[26] The IR spectra assignment was analyzed on the basis of atomic velocity autocorrelation functions, in which the vibrational quantum effects were ignored.[26] In this regard, Paesani and co-workers have developed empirical potential energy functions for liquid water and solutes.[61−63] Various approximate methods are available to account for the time-dependent nuclear quantum effects, including linearized semiclassical initial value representation (LSC-IVR),[64−66] centroid molecular dynamics,[13,67−73] and ring-polymer molecular dynamics.[72,74−78] One can, of course, solve numerically the vibrational Schrödinger equation.[13,67−73] Mancini and Bowman[50−53,79] employed diffusion Monte Carlo simulations to investigate the high-frequency fundamental modes of HCl–water clusters. Good agreement was observed between the calculated vibrational frequencies and experimental peak positions when the delocalized zero-point vibrational motion was taken into account.[50]

The IR signature of H_3O^+ in the dissociated configuration of $H_3O^+(H_2O)_3Cl^-$ was investigated using a vibrational configuration interaction (VCI) with the local monomer (LMon) potential energy surface,[79] providing peak positions and intensities. The VCI calculations employed eight states for each vibrational mode, coupled to up to four other modes, on 10G integration points per mode. Although these studies provided significant insights on mode coupling and peak positions of H_3O^+ for a single fixed water–Cl^- configuration, the method does not provide spectral line shape and is too time-consuming to obtain time-dependent frequencies in dynamics simulations.

Explicit quantum mechanical treatments of both the nuclear motion and the potential energy surface are required to understand the solute–solvent interaction dynamics in 1-D and 2-D vibrational spectroscopic experiments. In principle, path-integral molecular dynamics employing an on-the-fly QM potential can be used; however, the high computational costs limit its broad applications, especially when excitation involving higher vibrational states is investigated. In practice, empirical spectroscopic maps that relate the frequency change to the local electric field have been widely used. The method has been shown to be quite reliable for systems dominated by electrostatic interactions.[1−3,80,81] However, the electrostatics-based spectroscopic map does not fully take into account exchange and dispersion interactions, nor explicit polarization effects and charge transfer contributions. Thus, large deviations were found in simulations of N-methylacetamide (NMA) in $CDCl_3$ solution in which dispersion forces are dominant.[39] To this end, combined QM/MM methods, in which the probe molecule is treated explicitly by electronic structure theory, provide the most general, efficient, and systematic approach to represent the potential energy surface.[82,83] It also avoids the need to fit a secondary dipole moment surface that is typically inconsistent with the electrostatic properties of the empirical potential function.[1,4,13,79] The instantaneous vibrational energy levels can be determined by solving the vibrational Schrödinger equation for a given mode or coupled modes based on the QM/MM potential,[13,82] but the increased computational costs prevent it from being effectively used to obtain the frequency time correlation function (FTCF). Thus, it is useful to develop computationally efficient methods to accurately determine the time-dependent vibrational frequencies of a specific vibrational mode of a probe oscillator in solution and biological systems.

In this paper, we describe a perturbation approach to efficiently determine the instantaneous vibrational frequency of one or two specific target modes. The method is based on quantum vibrational perturbation (QVP) theory by means of potential-optimized discrete variable representation (PODVR).[84,85] The key in the QVP method is to estimate the vibrational energy shift of the solute (probe) molecule induced by interactions with the solvent environment without the need to solve the vibrational Schrödinger equation.[86,87] The QVP method incorporates nuclear quantum effects of the vibrational probe as well as the influence of dynamic fluctuations of the environment, and it can be applied to large molecular systems directly in molecular dynamics simulations with a combined QM/MM potential. The QVP method is illustrated and validated by an application to the small yet challenging HCl–water clusters to determine the IR spectra in the HCl stretching region.

2. METHOD

In the present QVP approach, the energy of each vibrational state of the oscillator is obtained by treating the solvent fluctuation as a perturbation, $\Delta H(Q,R)$, to the reference configuration $H^0(Q,R_0)$, where Q and R refer to solute and solvent coordinates, and R_0 is the coordinates at the referenced state. Consequently, the instantaneous transition frequency from the ground vibrational state (v = 0) to the first excited state (v = 1) for the mode of interest is given by

$$\omega_{10}(t) = \omega_{10}^{o} + \Delta\omega_{10}(t) \tag{1}$$

where ω_{10}^{o} is the vibrational frequency of the reference state, which is the minimum-energy structure of the ClH–OH_2 complex. In eq 1, the frequency shift $\Delta\omega_{10}(t)$ is related to the perturbation energies of the instantaneous structure at time t:

$$\Delta\omega_{10}(t) = \frac{\Delta V_1(t) - \Delta V_0(t)}{\hbar} \tag{2}$$

where $\Delta V_0(t)$ and $\Delta V_1(t)$ are the energy changes due to external perturbation for the ground and first excited states of the quantum oscillator in the bath of a given solvent configuration.

Specifically, we first solve the vibrational Schrödinger equation for the reference structure defined by $H^0(Q,R_0)$ to yield the vibrational wave functions φ_v, based on which the optimal number of PODVR points is obtained.[85,88] For the ClH–OH_2 complex, we found that just eight PODVR points are sufficient to obtain convergent energies and wave functions for the lowest three vibrational states (see Supporting Information). They are depicted in Figure 1. Then, we use perturbation theory to determine the energy shifts for each vibrational level relative to that of the reference state.

DOI: 10.1021/acs.jctc.6b00733
J. Chem. Theory Comput. 2017, 13, 191–201

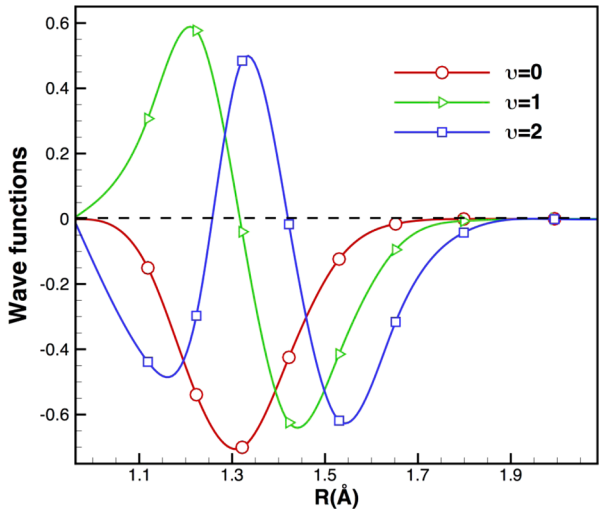

Figure 1. Computed vibrational wave functions of the ground and the first and second excited states of the HCl stretch mode in the optimized $HCl(H_2O)$ structure. Discrete variable representation (DVR) at the eight optimized grid points is indicated.

Importantly, the perturbation energies converge quickly, and the first order approximation (QVP1) is sufficient in the present test cases (see below).

In the PODVR basis $\{\chi^2(Q_i;R_0),\ i = 1-8\}$ over the discrete points along the HCl stretching mode for the reference state, R_0, the first order perturbation energy for state υ is given by

$$\Delta V_\upsilon(t) = \int dQ\ \Delta H(Q, R[t])|\varphi_\upsilon(Q; R_0)|^2 = \sum_{i=1}^{8} \Delta H(Q_i, R[t])\ c_{\upsilon i}^2 \chi^2(Q_i; R_0) \quad (3)$$

where Q_i is the coordinates of the ith PODVR point, $\{c_{\upsilon i}\}$ is the optimized and normalized coefficients for state υ in the PODVR basis, and $\Delta H(Q_i,R[t])$ is the perturbation energy corresponding to the chromophore at the discrete point Q_i and the instantaneous bath coordinates at $R[t]$ at time t. Equation 3 is based on the separation of inter- and intramolecular motions, which ignores the nuclear quantum mechanical effects on their coupling. This approximation is justified for situations in the present study (except when HCl dissociation occurs with four water molecules) and is valid for most applications in biological systems, where the vibrational frequency of the probe molecule is designed to clearly separate from the bath modes. Nevertheless, coupling to higher quanta of bath modes could be important and a procedure developed by Skinner and co-workers can be applied here to treat such situations.[12] In practice, $\Delta H(Q_i,R[t])$ can be evaluated using a combined QM/MM potential, or by a mixed fragmental QM model in which the solute and its nearest neighbors are described by a high-level theory embedded in the solvent environment to model long-range electrostatic effects.[89] In the latter case, short-range repulsion, dispersion, and charge transfer effects between the oscillator and solvent molecules in close proximity are naturally included in the QM model. For the present HCl–water clusters, the entire system is treated quantum-mechanically using two QM methods: M06-2X[90]/cc-pVTZ and CCSD(T)-F12B[91−93]/cc-pVTZ.

Equations 2 and 3 show that the present QVP1 method can be extremely efficient for computation of vibrational frequencies, which involve two weighted averages of the perturbation term. Thus, the computational cost is equivalent to that needed to determine the perturbation energy at the discrete points without explicitly solving the vibrational Schrödinger equation. The weighting coefficients in eq 3, defined by $\{\omega_i = c_{\upsilon i}\chi^2(Q_i,R_0),\ \upsilon = 1, 2\}$, are predetermined for the chromophore oscillator in the reference structure and optimized to represent the vibrational wave function in the PODVR method. Higher order perturbation terms can be used if greater computational accuracy is desired or becomes necessary.

To quantify convergence of the present perturbation strategy, we selected 40 structures from the molecular dynamical trajectory of $HCl(H_2O)$ at equal intervals and determined the exact vibrational frequencies by solving numerically the Schrödinger equation and those estimated by the QVPn method up to the fourth-order perturbation (n = 1–4). The results are compared in Figure 2 spanning a range of

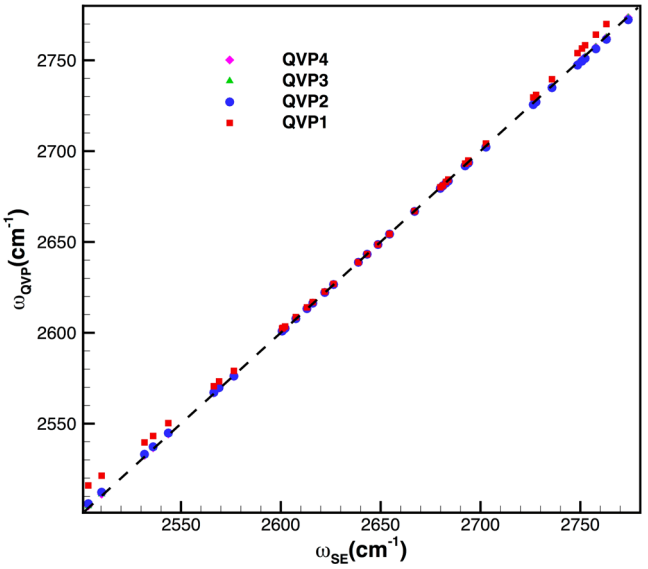

Figure 2. Correlation of the exact and the QVP vibrational frequencies for HCl in 40 complex structures from an ab initio molecular dynamics trajectory of the $H_2O\cdots HCl$ cluster using CCSD(T)-F12b/cc-pVTZ-F12. The exact results are obtained by solving the vibrational Schrödinger equation (abscissa) for each complex structure, whereas up to the fourth-order perturbation is used in the quantum vibrational perturbation (QVP) approach (ordinate). The black dashed line represents a perfect match.

vibrational frequency from 2500 to 2775 cm^{-1}. Figure 2 reveals that while the first-order perturbation approach QVP1 has good agreement with the exact result in the medium range of 2600–2700 cm^{-1}, increased deviations are observed at higher and lower frequencies with an average error of 3.0 cm^{-1}. As the order of perturbation increases, the computation accuracy increases sharply to root-mean-square deviations of 0.1, 0.04, and 0.04 cm^{-1} for the second-, third-, and fourth-order perturbation theory, respectively. However, higher vibration excited states are needed to obtain high-order perturbation energies, which translate to more discrete points in the PODVR evaluation. Since the frequency shifts are relatively large in the present test cases, the first-order perturbation QVP1 is used throughout.

DOI: 10.1021/acs.jctc.6b00733
J. Chem. Theory Comput. 2017, 13, 191–201

3. COMPUTATIONAL DETAILS

Born−Oppenheimer molecular dynamics simulations were performed using the meta-GGA M06-2X density functional theory with the cc-pVTZ basis for $HCl(H_2O)$ and using BLYP density functional theory augmented by dispersion corrections[88,89] for other cases with a plane wave basis set.[86,87,94] For each cluster, the dynamics simulations were carried out at 200 K for a total of 25 ps with an integration step of 30 au (0.72 fs). Additional details of the ab initio simulation procedure are given in the Supporting Information. For accuracy in the computed vibrational frequency, all the perturbation energies were determined using the M06-2X/cc-pVTZ and CCSD(T)-F12b/cc-pVTZ-F12 methods.[95] Basis set superposition errors (BSSE)[96] were corrected following the counterpoise scheme. Note that as the number of water increases in the $HCl(H_2O)_n$ clusters, HCl dissociation is observed when n is 4 as shown in Figure S1. This is consistent with the aggregation-induced dissociation mechanism[22,40] in previous simulations.[40,42−44,59,97]

For comparison, we have determined the linear absorption line shape by classical and mixed quantum/classical approaches.[1,4] In the classical approach, the line shape function is computed by Fourier transform of the autocorrelation function of the total molecular dipole moment from classical molecular dynamics simulations

$$I_{cl}(\omega) = Q_H(\omega) \int d\omega \left\langle \mu(0)\cdot\mu(t) \right\rangle e^{-i\omega t} \tag{4}$$

where $Q_H(\omega)$ is the harmonic quantum correction factor,[98,99] and the brackets specify a classical statistical mechanical average. In the mixed quantum/classical method,[1,4] where the HCl vibrational mode is treated quantum mechanically and all other degrees of freedom are modeled classically by molecular dynamics, a key quantity of interest is the $0 \rightarrow 1$ transition frequency and its dependence on the environment (eq 1). Then, within the Condon approximation, the magnitude of the vibrational transition moment is assumed to be independent of the bath fluctuations,[1] and the semiclassical absorption line shape can be written as

$$I_{sc}(\omega) = \int dt\, e^{-i\omega t} \left\langle e^{i\int_0^t d\tau \omega_{10}(\tau)} \right\rangle e^{-t/2T_1} \tag{5}$$

where T_1 is the vibrational energy relaxation time (224 fs), which is estimated following the work of Straub and coworkers[100−103] by computing the classical autocorrelation function of the force along the H−Cl bond. To evaluate the average in eq 5, the time evolutions for $\omega_{10}(t)$ are computed using the QVP1 method on the classical molecular dynamics trajectory. Equation 5 can be written in terms of cumulant expansion at the second-order truncation:

$$I_{cum}(\omega) = \int dt\, e^{-i(\omega - \langle\omega_{10}\rangle)t} e^{-\int_0^t d\tau (t-\tau) C(\tau)} e^{-t/2T_1} \tag{6}$$

where $\langle\omega_{10}\rangle$ is the average transition frequency and $C(t)$ is the frequency−frequency time-correlation function given by

$$C(t) = \langle \delta\omega(0)\, \delta\omega(t) \rangle \tag{7}$$

where

$$\delta\omega(t) = \omega_{10}(t) - \langle\omega_{10}\rangle$$

4. RESULTS AND DISCUSSION

We first present results on the hydrogen chloride−water clusters to demonstrate the performance of the quantum vibrational perturbation approach for determining on-the-fly vibrational frequencies. Here, the full system is represented by an electronic structure method. Then, we illustrate the applicability of the QVP method in condensed-phase simulations, making use of the carbonyl stretching mode of acetone in water as an example. In this case, combined QM/MM molecular dynamics simulations are performed to evaluate the perturbation energy using a semiempirical Hamiltonian.

4.1. HCl−Water Clusters. *$HCl(H_2O)$.* The computed and experimental IR spectra in the HCl stretching region of the bimolecular complex $HCl(H_2O)$ are given in Table 1 and displayed in Figure 3. In this discussion, we first address nuclear quantum effects on the computed frequency and then examine a hybrid procedure to increase the accuracy of the results, making use of the M06-2X trajectory. Figure 3a displays the line shape functions using the classical molecular dipole autocorrelation function (DAF) in blue (scaled by the harmonic quantum correction factor) and using eq 5 based on the QVP1 transition frequencies in green. The spectrum determined from the DAF shows a series of side peaks with an

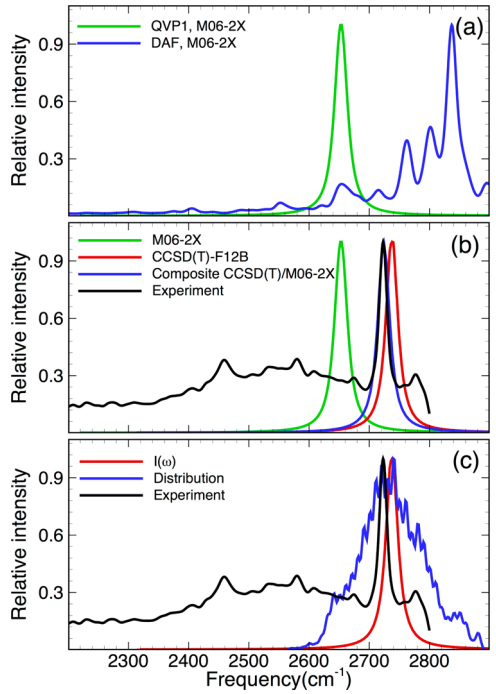

Figure 3. Normalized IR line shapes from experiment (black) and computations for the HCl stretching vibrational mode in the $HCl(H_2O)$ complex. (a) The spectrum obtained by Fourier transform of DAF (eq 4) is given in blue, and that from instantaneous QVP1 frequencies (eq 5) is displayed in green, both at the M06-2X/cc-pVTZ level. (b) Spectral line shapes determined by the second-cumulant expression based on the frequency−frequency time correlation function (eq 6) are shown at the CCSD(T)-F12b (red) and M06-2X (green) levels along with the composite of CCSD(T)-F12b frequency for the reference state and M06-2X frequency shifts (blue). (c) The distribution of computed H−Cl stretching frequency (blue) at the CCSD(T)-F12b level is illustrated along with the corresponding spectral line shape function (red) and the experimental spectrum (black).

DOI: 10.1021/acs.jctc.6b00733
J. Chem. Theory Comput. 2017, 13, 191−201

interval of about 50 cm^{-1}, attributed to the coupling with rotations of the water molecule about the H−Cl axis. This effect is not included in the instantaneous frozen-bath approximation in the QVP1 model. The maximum peak position from the QVP1 method is located at 2653 cm^{-1}, red-shifted by 185 cm^{-1} from the strongest peak position (2838 cm^{-1}) displayed on the spectrum based on the classical DAF (Table 1). Since M06-2X/cc-pVTZ was used in both approaches, consistent with the dynamic trajectory, the difference between the two methods is primarily due to nuclear quantum effects of the oscillator, which clearly have significant contributions to the computed vibrational frequencies in Figure 3a. Nevertheless, the full widths at half-maximum (fwhm) of the spectrum peak are similar from both methods (21 and 23 cm^{-1}, respectively).

Table 1. Computed HCl Stretching Vibrational Frequency ω_{Cl-H} and the Shift $\Delta\omega_{Cl-H}$ of the HCl(H_2O) Complex Using Harmonic Normal Mode Analysis (NMA), Fourier Transform of the Dipole Autocorrelation Function (DAF), and the Spectral Expansion (eq 6) of the Frequency-Frequency Time Correlation Function from the QVP1 Method, along with the Experimental Value (Vibrational Frequencies Given in cm^{-1})

	method	basis set	ω_{Cl-H}	$\Delta\omega_{Cl-H}$[a]
	HF	Q[b]	3033.0	309.5
NMA[15]	MP2	T[b]	2791.0	67.5
	CCSD(T)	D[b]	2782.0	58.5
DAF	M06-2X	cc-pVTZ	2837.6	114.1
QVP1	M06-2X	cc-pVTZ	2653.0	−70.5
	M06-2X/CCSD(T)-F12b	cc-pVTZ/cc-pVTZ-F12[c]	2724.8	1.3
	CCSD(T)-F12b	cc-pVTZ-F12	2737.6	14.1
EXP[15,16]			2723.5	

[a] $\Delta\omega_{Cl-H} = \omega_{Cl-H} - \omega_{exp}$. [b] aug-cc-pVXZ, X = D,T,Q. [c] M06-2X/cc-pVTZ+CCSD(T)-F12b/cc-pVTZ-F12.

Figure 3b compares the results obtained using three different electronic structure methods: M06-2X (green line), CCSD(T)-F12b (red line), and a composite of M06-2X spectral shift and the CCSD(T)-F12b frequency. In the latter approach, the CCSD(T)-F12b frequency for the reference state is used, but the spectral shift due to dynamic fluctuations of the solvent is determined at the M06-2X level using QVP1. We designate this method as CCSD(T)/M06 in Figure 3b, which significantly reduces the computational costs compared with that when the perturbation theory is also carried out at the CCSD(T)-F12b level. Figure 3b shows that the maximum peak position from QVP1 using CCSD(T)-F12b is only 14 cm^{-1} greater than the experimental value (2723.5 cm^{-1}).[16,17] The M06-2X frequency in the HCl(H_2O) complex is blue-shifted by 84.6 cm^{-1} from the coupled-cluster value, and this is mainly due to the difference in the reference state between the two methods: 80.6 cm^{-1} from 2650.5 cm^{-1} (CCSD(T)-F12b) to 2569.9 cm^{-1} (M06-2X). Thus, the solvatochromic shifts are not very sensitive to the quantum chemical models used, here, differing only by 4 cm^{-1} (84.6 vs 80.6 cm^{-1}). Clearly, it can be a major time-saving approach to use density functional theory to estimate the spectral shift, but the reference frequency value is evaluated using coupled cluster theory (eq 1) since the latter only needs to be computed once. As the computational cost of the QVP method is equivalent to that required to determine the perturbation energy at the discrete points, allowing the instantaneous vibrational frequency of the oscillator to be determined on-the-fly of dynamics simulations. Indeed, the composite approach, employing the CCSD(T) zeroth order frequency (reference state) and QVP1 frequency shift from M06-2X (blue curve in Figure 3b), yields a maximum peak position at 2725 cm^{-1}, only 13 cm^{-1} different from the CCSD(T)-F12b value (2738 cm^{-1}). Interestingly, the composite result is in better accord with experimental results than CCSD(T)-F12b, perhaps due to fortuitous error cancellations. Furthermore, the computed fwhm from the composite strategy is 21 cm^{-1}, also in good agreement with experimental results (18 cm^{-1}),[16,17] and consistent with pure CCSD(T)-F12b and M06-2X calculations. The agreement between theory and experimental results both in peak position and in line shape suggests that the QVP1 composite approach can be used for studying IR spectra of probe molecules in the condensed-phase and in biomolecular systems.

In Figure 3c, we compare the distribution of instantaneous vibrational frequencies (blue) computed along an MD trajectory with the line shape function (eq 6) determined at the CCSD(T)-F12b/cc-pVTZ-F12 level (red). Although the average peak positions are the same, the statistical distribution of the computed frequencies is clearly not an adequate approximation to the spectral line shape due to motion narrowing effects. Similar features were found in the study of HOD vibration in H_2O and in D_2O employing a polarizable empirical potential for water.[13]

The 2D pump−probe spectra for the HCl stretching vibration in HCl(H_2O) are computed using the instantaneous vibrational frequencies determined by the CCSD(T)/M06-2X composite strategy along with t_2 evolution (additional details are given in the SI). In Figure 4, the ω_1 axis represents the pump pulse, while the ω_3 axis specifies the probe pulse. The projection on ω_3 is the dynamical line shape both for the vibrational bands of the 1−0 resonance (red) and for the 2−1 resonance (blue). The 2D IR spectra are displayed in Figure 3 for t_2 waiting times of 0, 302, 504, and 705 fs. At t_2 = 0 fs, the spectrum is diagonally elongated and antidiagonally narrowed, which demonstrates the anisotropy of the two vibrational bands and indicates a strong correlation of the vibrational bands. The antidiagonal direction is broadened and the nodal slope (separating the positive region of the 1−0 resonance from the negative region of the 2−1 resonance in the 2D spectra and the slope lines are shown as the blue dashed lines in Figure 4) decreases as t_2 increases, indicating reduction of correlation. At t_2 = 705 fs, the nodal slope is closer to zero, where the coupling of the two vibrational bands vanishes.

The 2D IR spectra provide a direct measure of the anharmonicity of the probe mode. Figure 4 indicates that the anharmonic frequency shift from the QVP1 approach is 140 cm^{-1} for H−Cl stretching vibration in the HCl(H_2O) complex, which is the difference between the central frequencies at positive (red) and negative (blue) peak regions. In comparison with the anharmonic frequency shift of 104 cm^{-1} estimated for an isolated HCl molecule, hydrogen bonding interactions as well as dispersion contributions further increase anharmonicity in the HCl(H_2O) cluster. It is interesting to note that 1−0 and 2−1 transitions for the HCl stretching mode in HCl(H_2O) are red-shifted, respectively, by 161 and 197 cm^{-1} relative to an isolated HCl. Apparently, hydrogen bonding interactions have a greater effect on the higher vibrational energy levels than the ground state.

DOI: 10.1021/acs.jctc.6b00733
J. Chem. Theory Comput. 2017, 13, 191−201

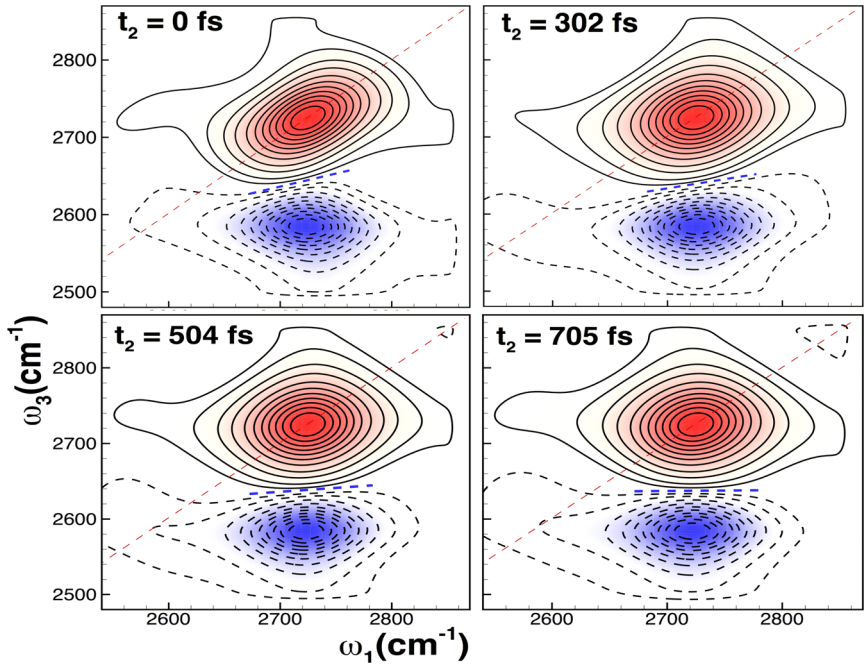

Figure 4. 2D pump−probe spectra of the HCl stretching vibration in the $HCl(H_2O)$ complex given at the evolution time t_2 equaling 0, 302, 504, and 705 fs, respectively. See text for specific details.

$(HCl)_2(H_2O)$. There are two HCl stretching vibrations in $(HCl)_2(H_2O)$. Here, we focus on the HCl stretching mode in which the hydrogen atom is hydrogen-bonded to the oxygen of water. Figure 5 depicts the line shape of the main peak, which is in good agreement with the experimental peak.[16,17] The peak position is centered at 2634 cm^{-1}, which is 54 cm^{-1} greater than the experimental value. The calculated line shape is similar to that from experimental results, indicated by the blue arrow of the spectrum in red. For this system, the time-dependent trajectories, including the $HCl(H_2O)_2$ cluster below, were sampled at the BLYP/plane wave level, but the vibrational frequencies were determined by using the composite QVP1 strategy.

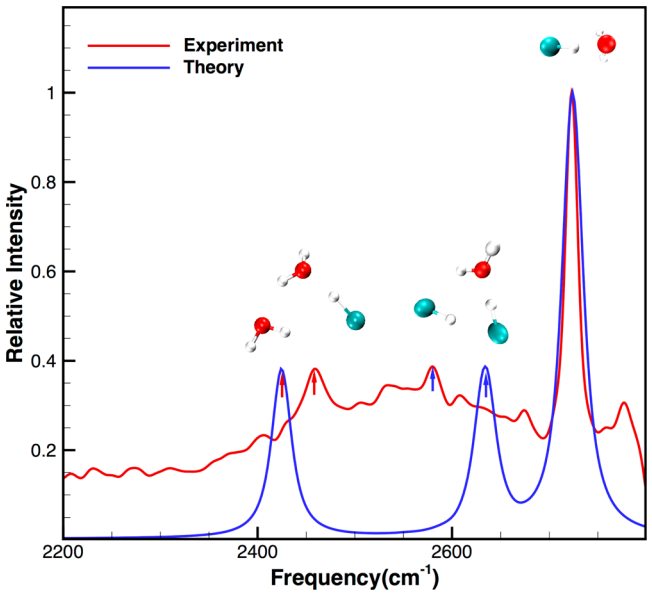

Figure 5. Experimental spectra and the overall computed HCl stretching vibrational spectra for a mixture of $(HCl)(H_2O)$, $(HCl)_2(H_2O)$, and $(HCl)(H_2O)_2$ clusters with weighting factors of 1, 0.41, and 0.46 for the relative intensities. The blue and red arrows specify the HCl stretching mode in the $(HCl)_2(H_2O)$ and $(HCl)(H_2O)_2$ clusters, respectively, and the strongest peaks correspond to that in the $HCl(H_2O)$ complex. The latter was sampled by M06-2X/cc-pVTZ, whereas the remaining systems were sampled using BLYP-D Born−Oppenheimer molecular dynamics simulations.

The present QVP method is applied to a single mode of interest, which ignores vibrational mode coupling in order to increase computational efficiency. For applications to biological systems, in which there is a vibrational frequency of the probe molecule (e.g., chromophores with triple bond or C−D stretch), the effect is expected to be small. However, because of the proximity of two similar HCl vibrations, mode coupling could be important. To address this question, we have determined the frequencies of both HCl molecules in the optimized $(HCl)_2(H_2O)$ complex (see Figure 5) by solving one-dimensional and two-dimensional vibrational Schrodinger equations, i.e., one based on the potential energy surface of independent modes and the second employing the full potential of the two modes, both at the M06-2X/cc-pVTZ level (Table 2). Mode coupling is included in the latter

Table 2. Computed H−Cl Stretching Vibrational Frequencies (cm^{-1}) for $(HCl)_2(H_2O)$ by Solving Two Independent One-Dimensional (E_{1D}) Schrodinger Equations and a Two-Dimensional (E_{2D}) Vibrational Schrodinger Equation[a]

Mode	E_{1D}	E_{2D}	$\Delta\nu$
Q_1	2617.0	2612.3	4.7
Q_2	2692.6	2693.7	−1.1

[a]The potential energy surfaces were determined using M06-2X/cc-pVTZ. Q_1 and Q_2 represent, respectively, the H−Cl stretch associated with the HCl molecule directly hydrogen-bonded to water and hydrogen-bonded to the probe HCl molecule (Figure 5).

DOI: 10.1021/acs.jctc.6b00733
J. Chem. Theory Comput. 2017, 13, 191−201

approach. It was found that the mode corresponding to the HCl molecule directly hydrogen-bonded to water is lowered by 4.7 cm^{-1} due to coupled interactions with the second HCl molecule, whereas the stretch frequency of the other HCl is enhanced by 1.1 cm^{-1}. Thus, the effect due to mode coupling is not significant in this case.

$HCl(H_2O)_2$. The peak position of the HCl stretching vibrational mode of the 1:2 cluster, illustrated in Figure 5, is found at 2424 cm^{-1}, which is close to the peak at 2460 cm^{-1} found experimentally.[16,17] The computed line shape for the $HCl(H_2O)_2$ complex is somewhat narrower than that from the experiment, highlighted by the red arrows in Figure 5.

Finally, we note that Figure 5 was constructed by summing up the individual HCl stretching vibrational spectra of the $(HCl)(H_2O)$, $(HCl)_2(H_2O)$, and $(HCl)(H_2O)_2$ clusters with weighting factors for relative intensities of 1, 0.41, and 0.46, respectively. Both the peak positions and line shapes are in reasonable agreement with the experimental spectra, which further support our assignments of those peaks as the HCl stretching mode in the $(HCl)(H_2O)$, $(HCl)_2(H_2O)$, and $(HCl)(H_2O)_2$ clusters, respectively. The molecular structures for the clusters, $(HCl)(H_2O)$, $(HCl)_2(H_2O)$, and $(HCl)(H_2O)_2$, are shown in Figure S2 along with key geometrical parameters indicated.

4.2. Acetone in Aqueous Solution. To illustrate the general applicability of the QVP method in condensed-phase simulations, we carried out "on-the-fly" vibrational frequency calculations for the carbonyl stretching mode of acetone in aqueous solution. QM/MM potential[54,104] is employed, in which the chromophore is approximated by the semiempirical Austin Model 1 (AM1)[105] Hamiltonian, and the solvent is represented by the TIP3P model for water. A single solute molecule is embedded in a cubic box of 467 water molecules using the isothermal−isobaric (NPT) ensemble at 25 °C and 1 atm. The time-step in the simulation is 1 fs, and a convergent QVP spectrum of C═O vibration is obtained using a 50 ps trajectory. All computations are carried out using CHARMM. Here, the instantaneous vibrational frequency of the carbonyl stretch in water is determined using the composite approach described in the previous section, where the reference state is determined at a high level of theory, whereas the perturbation energy is obtained at the combined QM/MM level to account for solvent effects. In particular, the C═O vibrational wave functions for the first three vibrational states of an isolated acetone molecule in the gas phase are determined using the potential energy curve from CCSD(T)-F12/cc-pVTZ-F12 calculations along the C═O normal mode coordinate. The 0 → 1 transition frequency is determined to be 1776 cm^{-1}, in reasonable agreement with the experimental value of 1738 cm^{-1} in the vapor phase, and the small difference of +38 cm^{-1} will be fully transferred to the solution result.

Figure 6 displays the computed vibrational spectra for the C═O stretching mode of acetone in water using the Fourier transform of the dipole autocorrelation function (DAF; blue curve) and that from the cumulant expansion of the QVP1 frequency fluctuation autocorrelation function (red curves), along with the experimental results (black curve).[57] The peak position at 1741 cm^{-1} from the QVP1 method represents a solvent-induced red shift of −35 cm^{-1}, which may be compared with a solvent effect of −41 cm^{-1}, corresponding to a maximum peak position at 1697 cm^{-1}. The agreement indicates that the AM1 model used in combined QM/MM simulations can capture the large bulk of solvation effects. In addition, the

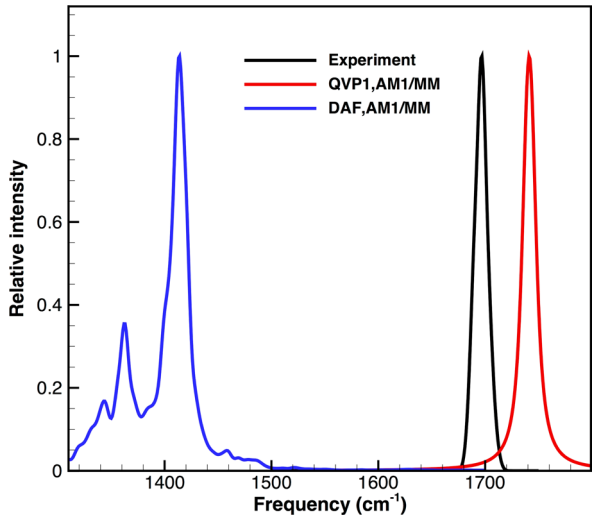

Figure 6. Experimental (black) and computed vibrational spectra of the carbonyl stretching region of acetone in water. The spectrum from the first-order quantum vibration perturbation (QVP1) calculation employing a composite of the CCSD(T) reference frequency and a QM(AM1)/MM perturbation potential is shown in red, and that from the Fourier transform of the molecular dipole autocorrelation function determined using AM1 directly in QM/MM simulations is given in blue.

calculated fwhm (14.8 cm^{-1}) is in good accord with the experiment (15.1 cm^{-1}).[57,58] On the other hand, the maximum peak position is found at 1414 cm^{-1} by Fourier transform of DAF, which is red-shifted by −30 cm^{-1} from the corresponding gas-phase value. The AM1 Hamiltonian severely underestimates the carbonyl stretch frequency of acetone by 294 cm^{-1} compared with experimental results, which is fully translated into the condensed-phase results by direct application of the molecular dipole autocorrelation function. Since the Fourier transform of DAF includes anharmonicity and captures the same solvent effect as that in the QVP1 calculations, the small difference of 5 cm^{-1} between the two methods is attributed to nuclear quantum effects. The difference between the QVP1 and DAF results also illustrates the use of the composite approach to effectively correct errors in the low-level QM/MM representation of the absolute vibrational frequency.

5. CONCLUSIONS

We have presented a nuclear quantum vibrational perturbation (QVP) method for efficiently determining the instantaneous vibrational frequency of a chromophore in molecular dynamics simulations. The QVP approach is a semiclassical approach that combines quantum mechanical treatment of nuclear motions of specific vibrational modes with classical dynamics simulations. The method treats intermolecular interactions as a perturbation to the vibrational Hamiltonian on a predefined reference state. Computational efficiency is achieved as a result of three key ingredients, including (a) the use of potential optimized discrete variable representation (PODVR) of the vibrational wave functions for all levels of interest, (b) the application of perturbation theory to evaluate the energy shifts due to solvent dynamic fluctuations, and (c) the representation of the potential energy surface by a combined QM/MM approach for condensed-phase and macromolecular systems. Furthermore, we found that first-order perturbation is sufficiently

DOI: 10.1021/acs.jctc.6b00733
J. Chem. Theory Comput. 2017, 13, 191−201

accurate for the present HCl−water cluster system, a small but challenging test case due to strong bond-dissociation character associated with the vibrational mode as well as hydrogen bonding interactions. The use of the PODVR representation and perturbation theory to determine the energy shifts avoids the need to solve the vibrational Schrödinger equation. Thus, the computational cost of the QVP method is equivalent to that needed to determine the potential energies at the PODVR points. The use of a combined QM/MM approach incorporates naturally the effects of solvent dynamics on the potential energy surface, which can be systematically improved in accuracy and is computationally efficient. It also avoids the need to develop empirical potential energy surface and offer the accompanying dipole moment surface for every new system. Since time-dependent vibrational frequencies can be determined on the fly in molecular dynamics simulations, the mode-specific linear and 2D-IR spectra can be extracted from the frequency time correlation function. Although the QVP method is validated using the HCl−water clusters, we emphasize that the approach can easily be extended to macromolecular systems since the perturbation theory calculation is only concerned with one-electron integrals in a combined QM/MM potential. Thus, as long as it is possible to carry out QM/MM simulations at the desired QM level, the QVP1 method can be used to determine on-the-fly vibrational frequencies at the same or better accuracy.

Intra- and intermolecular mode coupling can be important, but it is not specifically included in the present QVP method except the effect due to intermolecular interactions in the QM/MM potential energy surface. This is a subject of future research, though one can straightforwardly extend the present single mode approach to two or more coupled modes (as illustrated in the text), making use of the PODVR numerical method. Intramolecular (and intermolecular) mode-coupling can also be treated by using vibrational configuration interaction (VCI) as implemented in the MULTIMODE program, but the computational costs are prohibitive for computation of time-dependent vibrational frequencies. A linear scaling strategy is clearly desired.

To further reduce computational costs, we examined a hybrid, or composite strategy that can yield accurate peak position and line shape. In this scheme, the reference-state vibrational frequency (eq 1) is determined with a highly accurate method only once, but the vibrational frequency shifts at each instantaneous configuration along the MD trajectory are evaluated using the QVP method with a lower-level QM/MM potential. In the HCl−water cluster test cases, we compared the spectral result determined by using CCSD(T)-F12b on the entire system with that from the hybrid strategy with CCSD(T)-F12b reference frequency and M06-2X frequency shift. The agreement is very good, especially considering the tremendous cost-saving. Importantly, the inclusion of nuclear quantum effects, either using the semiclassical (eq 5) or cumulant expansion (eq 6) algorithm, has a large effect on the computed spectra and is found to be in better agreement with experiment than that obtained by Fourier transform of the classical dipole autocorrelation function. We found that anharmonicity in the H−Cl stretch is significant and has a large solvent effect in the relaxation process exhibited in the computed 2D-IR spectra. To illustrate the general applicability, solvent effects on the carbonyl stretch of acetone in water were determined using QVP1 with a dual-level approach using the CCSD(T) results as the reference state coupled with combined QM(AM1)/MM simulations to account for solute−solvent interactions. The computed solvent-induced spectral shifts are in accord with experimental results. The present QVP method complements other computational approaches, including path integral-based molecular dynamics, and represents a major improvement over the electrostatics-based spectroscopic mapping procedures.

■ ASSOCIATED CONTENT

Supporting Information

The Supporting Information is available free of charge on the ACS Publications website at DOI: 10.1021/acs.jctc.6b00733.

The convergent test of HCl stretch vibration within $HClH_2O$ complex, the perturbation approach test, ab initio molecular simulation setup, the response function of rephrasing and non-rephrasing processes (PDF)

■ AUTHOR INFORMATION

Corresponding Authors

*E-mail: gao@jialigao.org.
*E-mail: Prof_huili@jlu.edu.cn.

ORCID

Jiali Gao: 0000-0003-0106-7154

Notes

The authors declare no competing financial interest.

■ ACKNOWLEDGMENTS

We thank Martin A. Suhm and Michal Fárník for providing the raw experimental data. This research has been supported by grants from the National Natural Science Foundation of China (Grant Nos. 21273094 and 21533003), Program for New Century Excellent Talents in University and the National Institutes of Health (Grant No. GM46376).

■ REFERENCES

(1) Skinner, J. L.; Pieniazek, P. A.; Gruenbaum, S. M. Vibrational Spectroscopy of Water at Interfaces. *Acc. Chem. Res.* **2012**, *45*, 93−100.
(2) Fried, S. D.; Boxer, S. G. Measuring Electric Fields and Noncovalent Interactions Using the Vibrational Stark Effect. *Acc. Chem. Res.* **2015**, *48*, 998−1006.
(3) Fried, S. D.; Bagchi, S.; Boxer, S. G. Extreme electric fields power catalysis in the active site of ketosteroid isomerase. *Science* **2014**, *346*, 1510−1514.
(4) Kim, H.; Cho, M. Infrared Probes for Studying the Structure and Dynamics of Biomolecules. *Chem. Rev.* **2013**, *113*, 5817−5847.
(5) Reppert, M.; Tokmakoff, A. Electrostatic frequency shifts in amide I vibrational spectra: Direct parameterization against experiment. *J. Chem. Phys.* **2013**, *138*, 134116.
(6) Jeon, J.; Yang, S.; Choi, J.-H.; Cho, M. Computational Vibrational Spectroscopy of Peptides and Proteins in One and Two Dimensions. *Acc. Chem. Res.* **2009**, *42*, 1280−1289.
(7) Rosenfeld, D. E.; Gengeliczki, Z.; Smith, B. J.; Stack, T. D. P.; Fayer, M. D. Structural Dynamics of a Catalytic Monolayer Probed by Ultrafast 2D IR Vibrational Echoes. *Science* **2011**, *334*, 634−639.
(8) Culik, R. M.; Jo, H.; DeGrado, W. F.; Gai, F. Using Thioamides To Site-Specifically Interrogate the Dynamics of Hydrogen Bond Formation in β-Sheet Folding. *J. Am. Chem. Soc.* **2012**, *134*, 8026−8029.
(9) Tabor, D. P.; Kusaka, R.; Walsh, P. S.; Zwier, T. S.; Sibert, E. L. Local Mode Approach to OH Stretch Spectra of Benzene−(H2O)n Clusters, n = 2−7. *J. Phys. Chem. A* **2015**, *119*, 9917−9930.
(10) Choi, J.-H.; Kwak, K.-W.; Cho, M. Computational Infrared and Two-Dimensional Infrared Photon Echo Spectroscopy of Both Wild-

Type and Double Mutant Myoglobin-CO Proteins. *J. Phys. Chem. B* **2013**, *117*, 15462−15478.
(11) Cho, M. Coherent Two-Dimensional Optical Spectroscopy. *Chem. Rev.* **2008**, *108*, 1331−1418.
(12) Skinner, J. L.; Auer, B. M.; Lin, Y.-S. In *Adv. Chem. Phys.*; John Wiley & Sons, Inc.: 2008; pp 59−103.
(13) Paesani, F.; Xantheas, S. S.; Voth, G. A. Infrared Spectroscopy and Hydrogen-Bond Dynamics of Liquid Water from Centroid Molecular Dynamics with an Ab Initio-Based Force Field. *J. Phys. Chem. B* **2009**, *113*, 13118−13130.
(14) Lai, Z.; Preketes, N. K.; Mukamel, S.; Wang, J. Monitoring the Folding of Trp-Cage Peptide by Two-Dimensional Infrared (2DIR) Spectroscopy. *J. Phys. Chem. B* **2013**, *117*, 4661−4669.
(15) Lai, Z.; Preketes, N. K.; Jiang, J.; Mukamel, S.; Wang, J. Two-Dimensional Infrared (2DIR) Spectroscopy of the Peptide Beta3s Folding. *J. Phys. Chem. Lett.* **2013**, *4*, 1913−1917.
(16) Weimann, M.; Farnik, M.; Suhm, M. A. A first glimpse at the acidic proton vibrations in HCl−water clusters via supersonic jet FTIR spectroscopy. *Phys. Chem. Chem. Phys.* **2002**, *4*, 3933−3937.
(17) Fárník, M.; Weimann, M.; Suhm, M. A. Acidic protons before take-off: A comparative jet Fourier transform infrared study of small HCl− and HBr−solvent complexes. *J. Chem. Phys.* **2003**, *118*, 10120−10136.
(18) Huneycutt, A. J.; Stickland, R. J.; Hellberg, F.; Saykally, R. J. Infrared cavity ringdown spectroscopy of acid−water clusters: HCl−H2O,DCl−D2O, and DCl−(D2O)2. *J. Chem. Phys.* **2003**, *118*, 1221−1229.
(19) Ortlieb, M.; Birer, Ö.; Letzner, M.; Schwaab, G. W.; Havenith, M. Observation of Rovibrational Transitions of HCl, (HCl)2, and H2O−HCl in Liquid Helium Nanodroplets†. *J. Phys. Chem. A* **2007**, *111*, 12192−12199.
(20) Skvortsov, D.; Lee, S. J.; Choi, M. Y.; Vilesov, A. F. Hydrated HCl Clusters, HCl(H2O)1−3, in Helium Nanodroplets: Studies of Free OH Vibrational Stretching Modes†. *J. Phys. Chem. A* **2009**, *113*, 7360−7365.
(21) Zwier, T. S. Squeezing the Water Out of HCl(aq). *Science* **2009**, *324*, 1522−1523.
(22) Flynn, S. D.; Skvortsov, D.; Morrison, A. M.; Liang, T.; Choi, M. Y.; Douberly, G. E.; Vilesov, A. F. Infrared Spectra of HCl−H2O Clusters in Helium Nanodroplets. *J. Phys. Chem. Lett.* **2010**, *1*, 2233−2238.
(23) Morrison, A. M.; Flynn, S. D.; Liang, T.; Douberly, G. E. Infrared Spectroscopy of (HCl)m(H2O)n Clusters in Helium Nanodroplets: Definitive Assignments in the HCl Stretch Region. *J. Phys. Chem. A* **2010**, *114*, 8090−8098.
(24) Talukdar, R. K.; Burkholder, J. B.; Roberts, J. M.; Portmann, R. W.; Ravishankara, A. R. Heterogeneous Interaction of N2O5 with HCl Doped H2SO4 under Stratospheric Conditions: ClNO2 and Cl2 Yields. *J. Phys. Chem. A* **2012**, *116*, 6003−6014.
(25) Guggemos, N.; Slavíček, P.; Kresin, V. V. Electric Dipole Moments of Nanosolvated Acid Molecules in Water Clusters. *Phys. Rev. Lett.* **2015**, *114*, 043401.
(26) Lin, W.; Paesani, F. Infrared Spectra of HCl(H2O)n Clusters from Semiempirical Born−Oppenheimer Molecular Dynamics Simulations. *J. Phys. Chem. A* **2015**, *119*, 4450−4456.
(27) Samanta, A. K.; Wang, Y.; Mancini, J. S.; Bowman, J. M.; Reisler, H. Energetics and Predissociation Dynamics of Small Water, HCl, and Mixed HCl−Water Clusters. *Chem. Rev.* **2016**, *116*, 4913.
(28) Packer, M. J.; Clary, D. C. Interaction of HCl with water clusters: (H2O)nHCl, n = 1−3. *J. Phys. Chem.* **1995**, *99*, 14323−14333.
(29) Lee, C.; Sosa, C.; Planas, M.; Novoa, J. J. A theoretical study of the ionic dissociation of HF, HCl, and H2S in water clusters. *J. Chem. Phys.* **1996**, *104*, 7081−7085.
(30) Planas, M.; Lee, C.; Novoa, J. J. Kinetics of the Proton Transfer in X···(H2O)4 Clusters (X = H2O, NH3, H2S, and HCl): Evidence of a Concerted Mechanism. *J. Phys. Chem.* **1996**, *100*, 16495−16501.
(31) Estrin, D. o. A.; Kohanoff, J.; Laria, D. H.; Weht, R. O. Hybrid quantum and classical mechanical Monte Carlo simulations of the interaction of hydrogen chloride with solid water clusters. *Chem. Phys. Lett.* **1997**, *280*, 280−286.
(32) Re, S.; Osamura, Y.; Suzuki, Y.; Schaefer, H. F. Structures and stability of hydrated clusters of hydrogen chloride, HCl(H2O)n,n = 1−5. *J. Chem. Phys.* **1998**, *109*, 973−977.
(33) Bacelo, D. E.; Binning, R. C.; Ishikawa, Y. Ab Initio Monte Carlo Simulated Annealing Study of HCl(H2O)n (n = 3, 4) Clusters. *J. Phys. Chem. A* **1999**, *103*, 4631−4640.
(34) Chaban, G. M.; Gerber, R. B.; Janda, K. C. Transition from Hydrogen Bonding to Ionization in (HCl)n(NH3)n and (HCl)n-(H2O)n Clusters: Consequences for Anharmonic Vibrational Spectroscopy. *J. Phys. Chem. A* **2001**, *105*, 8323−8332.
(35) Milet, A.; Struniewicz, C.; Moszynski, R.; Wormer, P. E. S. Theoretical study of the protolytic dissociation of HCl in water clusters. *J. Chem. Phys.* **2001**, *115*, 349−356.
(36) Devlin, J. P.; Uras, N.; Sadlej, J.; Buch, V. Discrete stages in the solvation and ionization of hydrogen chloride adsorbed on ice particles. *Nature* **2002**, *417*, 269−271.
(37) Odde, S.; Mhin, B. J.; Lee, S.; Lee, H. M.; Kim, K. S. Dissociation chemistry of hydrogen halides in water. *J. Chem. Phys.* **2004**, *120*, 9524−9535.
(38) Sillanpää, A.; Laasonen, K. Car−Parrinello Molecular Dynamics Study of DCl Hydrate Crystals. *ChemPhysChem* **2005**, *6*, 1879−1883.
(39) la Cour Jansen, T.; Knoester, J. A transferable electrostatic map for solvation effects on amide I vibrations and its application to linear and two-dimensional spectroscopy. *J. Chem. Phys.* **2006**, *124*, 044502.
(40) Gutberlet, A.; Schwaab, G.; Birer, Ö.; Masia, M.; Kaczmarek, A.; Forbert, H.; Havenith, M.; Marx, D. Aggregation-Induced Dissociation of HCl(H2O)4 Below 1 K: The Smallest Droplet of Acid. *Science* **2009**, *324*, 1545−1548.
(41) Takayanagi, T.; Takahashi, K.; Kakizaki, A.; Shiga, M.; Tachikawa, M. Path-integral molecular dynamics simulations of hydrated hydrogen chloride cluster HCl(H2O)4 on a semiempirical potential energy surface. *Chem. Phys.* **2009**, *358*, 196−202.
(42) Sugawara, S.; Yoshikawa, T.; Takayanagi, T.; Tachikawa, M. Theoretical study on mechanisms of structural rearrangement and ionic dissociation in the HCl(H2O)4 cluster with path-integral molecular dynamics simulations. *Chem. Phys. Lett.* **2011**, *501*, 238−244.
(43) Walewski, Ł.; Forbert, H.; Marx, D. Quantum Induced Bond Centering in Microsolvated HCl: Solvent Separated versus Contact Ion Pairs. *J. Phys. Chem. Lett.* **2011**, *2*, 3069−3074.
(44) Walewski, Ł.; Forbert, H.; Marx, D. Revealing the Subtle Interplay of Thermal and Quantum Fluctuation Effects on Contact Ion Pairing in Microsolvated HCl. *ChemPhysChem* **2013**, *14*, 817−826.
(45) Masia, M.; Forbert, H.; Marx, D. Connecting Structure to Infrared Spectra of Molecular and Autodissociated HCl−Water Aggregates†. *J. Phys. Chem. A* **2007**, *111*, 12181−12191.
(46) Ndongmouo, U. F. T.; Lee, M. S.; Rousseau, R.; Baletto, F.; Scandolo, S. Finite-Temperature Effects on the Stability and Infrared Spectra of HCl(H2O)6 Clusters†. *J. Phys. Chem. A* **2007**, *111*, 12810−12815.
(47) Daniel Boese, A.; Forbert, H.; Masia, M.; Tekin, A.; Marx, D.; Jansen, G. Constructing simple yet accurate potentials for describing the solvation of HCl/water clusters in bulk helium and nanodroplets. *Phys. Chem. Chem. Phys.* **2011**, *13*, 14550−14564.
(48) Hassanali, A. A.; Cuny, J.; Ceriotti, M.; Pickard, C. J.; Parrinello, M. The Fuzzy Quantum Proton in the Hydrogen Chloride Hydrates. *J. Am. Chem. Soc.* **2012**, *134*, 8557−8569.
(49) Lin, W.; Paesani, F. Systematic Study of Structural and Thermodynamic Properties of HCl(H_2O)[sub:n] Clusters from Semiempirical Replica Exchange Simulations. *J. Phys. Chem. A* **2013**, *117*, 7131−7141.
(50) Mancini, J. S.; Bowman, J. M. Communication: A new ab initio potential energy surface for HCl−H2O, diffusion Monte Carlo calculations of D0 and a delocalized zero-point wavefunction. *J. Chem. Phys.* **2013**, *138*, 121102.

DOI: 10.1021/acs.jctc.6b00733
J. Chem. Theory Comput. 2017, 13, 191−201

(51) Mancini, J. S.; Bowman, J. M. Effects of Zero-Point Delocalization on the Vibrational Frequencies of Mixed HCl and Water Clusters. *J. Phys. Chem. Lett.* **2014**, *5*, 2247−2253.
(52) Mancini, J. S.; Bowman, J. M. A New Many-Body Potential Energy Surface for HCl Clusters and Its Application to Anharmonic Spectroscopy and Vibration−Vibration Energy Transfer in the HCl Trimer. *J. Phys. Chem. A* **2014**, *118*, 7367−7374.
(53) Mancini, J. S.; Samanta, A. K.; Bowman, J. M.; Reisler, H. Experiment and Theory Elucidate the Multichannel Predissociation Dynamics of the HCl Trimer: Breaking Up Is Hard To Do. *J. Phys. Chem. A* **2014**, *118*, 8402−8410.
(54) Gao, J. In *Reviews in Computational Chemistry*; Lipkowitz, K. B., Boyd, D. B., Eds.; VCH: New York, 1995; Vol. 7, pp 119−185.
(55) Dong, A.; Huang, P.; Caughey, W. S. Protein secondary structures in water from second-derivative amide I infrared spectra. *Biochemistry* **1990**, *29*, 3303−3308.
(56) Krimm, S.; Bandekar, J. In *Adv. Protein Chem.*; Anfinsen, C. B., Edsall, J., Richards, F., Eds.; Academic Press: 1986; Vol. *38*, pp 181−364.
(57) Haldar, T.; Bagchi, S. Electrostatic Interactions Are Key to C═O n-π^* Shifts: An Experimental Proof. *J. Phys. Chem. Lett.* **2016**, *7*, 2270−2275.
(58) Groenewold, G. S.; Gianotto, A. K.; Cossel, K. C.; Van Stipdonk, M. J.; Oomens, J.; Polfer, N.; Moore, D. T.; de Jong, W. A.; McIlwain, M. E. Mid-infrared vibrational spectra of discrete acetone-ligated cerium hydroxide cations. *Phys. Chem. Chem. Phys.* **2007**, *9*, 596−606.
(59) Letzner, M.; Gruen, S.; Habig, D.; Hanke, K.; Endres, T.; Nieto, P.; Schwaab, G.; Walewski, Ł.; Wollenhaupt, M.; Forbert, H.; Marx, D.; Havenith, M. High resolution spectroscopy of HCl−water clusters: IR bands of undissociated and dissociated clusters revisited. *J. Chem. Phys.* **2013**, *139*, 154304.
(60) McNeill, V. F.; Loerting, T.; Geiger, F. M.; Trout, B. L.; Molina, M. J. Hydrogen chloride-induced surface disordering on ice. *Proc. Natl. Acad. Sci. U. S. A.* **2006**, *103*, 9422−9427.
(61) Babin, V.; Leforestier, C.; Paesani, F. Development of a "First Principles" Water Potential with Flexible Monomers: Dimer Potential Energy Surface, VRT Spectrum, and Second Virial Coefficient. *J. Chem. Theory Comput.* **2013**, *9*, 5395−5403.
(62) Babin, V.; Medders, G. R.; Paesani, F. Development of a "First Principles" Water Potential with Flexible Monomers. II: Trimer Potential Energy Surface, Third Virial Coefficient, and Small Clusters. *J. Chem. Theory Comput.* **2014**, *10*, 1599−1607.
(63) Medders, G. R.; Babin, V.; Paesani, F. Development of a "First-Principles" Water Potential with Flexible Monomers. III. Liquid Phase Properties. *J. Chem. Theory Comput.* **2014**, *10*, 2906−2910.
(64) Sun, X.; Wang, H.; Miller, W. H. Semiclassical theory of electronically nonadiabatic dynamics: Results of a linearized approximation to the initial value representation. *J. Chem. Phys.* **1998**, *109*, 7064−7074.
(65) Wang, H.; Sun, X.; Miller, W. H. Semiclassical approximations for the calculation of thermal rate constants for chemical reactions in complex molecular systems. *J. Chem. Phys.* **1998**, *108*, 9726−9736.
(66) Liu, J.; Miller, W. H. Linearized semiclassical initial value time correlation functions using the thermal Gaussian approximation: Applications to condensed phase systems. *J. Chem. Phys.* **2007**, *127*, 114506.
(67) Cao, J.; Voth, G. A. The formulation of quantum statistical mechanics based on the Feynman path centroid density. II. Dynamical properties. *J. Chem. Phys.* **1994**, *100*, 5106−5117.
(68) Cao, J.; Voth, G. A. The formulation of quantum statistical mechanics based on the Feynman path centroid density. III. Phase space formalism and analysis of centroid molecular dynamics. *J. Chem. Phys.* **1994**, *101*, 6157−6167.
(69) Cao, J.; Voth, G. A. The formulation of quantum statistical mechanics based on the Feynman path centroid density. IV. Algorithms for centroid molecular dynamics. *J. Chem. Phys.* **1994**, *101*, 6168−6183.
(70) Cao, J.; Voth, G. A. The formulation of quantum statistical mechanics based on the Feynman path centroid density. I. Equilibrium properties. *J. Chem. Phys.* **1994**, *100*, 5093−5105.
(71) Cao, J.; Voth, G. A. The formulation of quantum statistical mechanics based on the Feynman path centroid density. V. Quantum instantaneous normal mode theory of liquids. *J. Chem. Phys.* **1994**, *101*, 6184−6192.
(72) Rossi, M.; Liu, H.; Paesani, F.; Bowman, J.; Ceriotti, M. Communication: On the consistency of approximate quantum dynamics simulation methods for vibrational spectra in the condensed phase. *J. Chem. Phys.* **2014**, *141*, 181101.
(73) Medders, G. R.; Paesani, F. Infrared and Raman Spectroscopy of Liquid Water through "First-Principles" Many-Body Molecular Dynamics. *J. Chem. Theory Comput.* **2015**, *11*, 1145−1154.
(74) Craig, I. R.; Manolopoulos, D. E. Quantum statistics and classical mechanics: Real time correlation functions from ring polymer molecular dynamics. *J. Chem. Phys.* **2004**, *121*, 3368−3373.
(75) Craig, I. R.; Manolopoulos, D. E. Chemical reaction rates from ring polymer molecular dynamics. *J. Chem. Phys.* **2005**, *122*, 084106.
(76) Craig, I. R.; Manolopoulos, D. E. A refined ring polymer molecular dynamics theory of chemical reaction rates. *J. Chem. Phys.* **2005**, *123*, 034102.
(77) Braams, B. J.; Manolopoulos, D. E. On the short-time limit of ring polymer molecular dynamics. *J. Chem. Phys.* **2006**, *125*, 124105.
(78) Rossi, M.; Ceriotti, M.; Manolopoulos, D. E. How to remove the spurious resonances from ring polymer molecular dynamics. *J. Chem. Phys.* **2014**, *140*, 234116.
(79) Mancini, J. S.; Bowman, J. M. Isolating the spectral signature of H3O+ in the smallest droplet of dissociated HCl acid. *Phys. Chem. Chem. Phys.* **2015**, *17*, 6222−6226.
(80) Ham, S.; Kim, J.-H.; Lee, H.; Cho, M. Correlation between electronic and molecular structure distortions and vibrational properties. II. Amide I modes of NMA−nD2O complexes. *J. Chem. Phys.* **2003**, *118*, 3491−3498.
(81) Hayashi, T.; Zhuang, W.; Mukamel, S. Electrostatic DFT Map for the Complete Vibrational Amide Band of NMA. *J. Phys. Chem. A* **2005**, *109*, 9747−9759.
(82) Garcia-Viloca, M.; Nam, K.; Alhambra, C.; Gao, J. Solvent and Protein Effects on the Vibrational Frequency Shift and Energy Relaxation of the Azide Ligand in Carbonic Anhydrase. *J. Phys. Chem. B* **2004**, *108*, 13501−13512.
(83) Błasiak, B.; Cho, M. Vibrational solvatochromism. II. A first-principle theory of solvation-induced vibrational frequency shift based on effective fragment potential method. *J. Chem. Phys.* **2014**, *140*, 164107.
(84) Echave, J.; Clary, D. C. Potential optimized discrete variable representation. *Chem. Phys. Lett.* **1992**, *190*, 225−230.
(85) Colbert, D. T.; Miller, W. H. A novel discrete variable representation for quantum mechanical reactive scattering via the S-matrix Kohn method. *J. Chem. Phys.* **1992**, *96*, 1982.
(86) Li, H.; Blinov, N.; Roy, P.-N.; Le Roy, R. J. Path-integral Monte Carlo simulation of ν3 vibrational shifts for CO2 in (He)n clusters critically tests the He−CO2 potential energy surface. *J. Chem. Phys.* **2009**, *130*, 144305.
(87) Li, H.; Ma, Y.-T. An intramolecular vibrationally excited intermolecular potential for He−OCS: Globally tested by simulation of vibrational shifts for OCS in HeN N = 1 − 100 Clusters. *J. Chem. Phys.* **2012**, *137*, 234310.
(88) Coxon, J. A.; Hajigeorgiou, P. G. The Radial Hamiltonians for the X1Σ+ and B1Σ+ States of HCl. *J. Mol. Spectrosc.* **2000**, *203*, 49−64.
(89) Wang, Y.; Sosa, C. P.; Cembran, A.; Truhlar, D. G.; Gao, J. Multilevel X-Pol: A Fragment-Based Method with Mixed Quantum Mechanical Representations of Different Fragments. *J. Phys. Chem. B* **2012**, *116*, 6781−6788.
(90) Zhao, Y.; Truhlar, D. The M06 suite of density functionals for main group thermochemistry, thermochemical kinetics, noncovalent interactions, excited states, and transition elements: two new functionals and systematic testing of four M06-class functionals and 12 other functionals. *Theor. Chem. Acc.* **2008**, *120*, 215−241.

DOI: 10.1021/acs.jctc.6b00733
J. Chem. Theory Comput. 2017, 13, 191−201

(91) Raghavachari, K.; Trucks, G. W.; Pople, J. A.; Head-Gordon, M. A fifth-order perturbation comparison of electron correlation theories. *Chem. Phys. Lett.* **1989**, *157*, 479−483.
(92) Hättig, C.; Klopper, W.; Köhn, A.; Tew, D. P. Explicitly Correlated Electrons in Molecules. *Chem. Rev.* **2012**, *112*, 4−74.
(93) Kong, L.; Bischoff, F. A.; Valeev, E. F. Explicitly Correlated R12/F12 Methods for Electronic Structure. *Chem. Rev.* **2012**, *112*, 75−107.
(94) Grimme, S. Semiempirical GGA-type density functional constructed with a long-range dispersion correction. *J. Comput. Chem.* **2006**, *27*, 1787−1799.
(95) Valiev, M.; Bylaska, E. J.; Govind, N.; Kowalski, K.; Straatsma, T. P.; Van Dam, H. J. J.; Wang, D.; Nieplocha, J.; Apra, E.; Windus, T. L.; de Jong, W. A. NWChem: A comprehensive and scalable open-source solution for large scale molecular simulations. *Comput. Phys. Commun.* **2010**, *181*, 1477−1489.
(96) Boys, S. F.; Bernardi, F. The calculation of small molecular interactions by the differences of separate total energies. Some procedures with reduced errors. *Mol. Phys.* **1970**, *19*, 553−566.
(97) Forbert, H.; Masia, M.; Kaczmarek-Kedziera, A.; Nair, N. N.; Marx, D. Aggregation-Induced Chemical Reactions: Acid Dissociation in Growing Water Clusters. *J. Am. Chem. Soc.* **2011**, *133*, 4062−4072.
(98) Bader, J. S.; Berne, B. J. Quantum and classical relaxation rates from classical simulations. *J. Chem. Phys.* **1994**, *100*, 8359−8366.
(99) Skinner, J. L.; Park, K. Calculating Vibrational Energy Relaxation Rates from Classical Molecular Dynamics Simulations: Quantum Correction Factors for Processes Involving Vibration−Vibration Energy Transfer†. *J. Phys. Chem. B* **2001**, *105*, 6716−6721.
(100) Sagnella, D. E.; Straub, J. E.; Jackson, T. A.; Lim, M.; Anfinrud, P. A. Vibrational population relaxation of carbon monoxide in the heme pocket of photolyzed carbonmonoxy myoglobin: Comparison of time-resolved mid-IR absorbance experiments and molecular dynamics simulations. *Proc. Natl. Acad. Sci. U. S. A.* **1999**, *96*, 14324−14329.
(101) Sagnella, D. E.; Straub, J. E. A Study of Vibrational Relaxation of B-State Carbon Monoxide in the Heme Pocket of Photolyzed Carboxymyoglobin. *Biophys. J.* **1999**, *77*, 70−84.
(102) Bu, L.; Straub, J. E. Simulating Vibrational Energy Flow in Proteins: Relaxation Rate and Mechanism for Heme Cooling in Cytochrome c. *J. Phys. Chem. B* **2003**, *107*, 12339−12345.
(103) Bu, L.; Straub, J. E. Vibrational Frequency Shifts and Relaxation Rates for a Selected Vibrational Mode in Cytochrome c. *Biophys. J.* **2003**, *85*, 1429−1439.
(104) Gao, J.; Thompson, M. A. *Combined Quantum Mechanical and Molecular Mechanical Methods*; American Chemical Society: Washington, DC, 1998; Vol. *712*.
(105) Dewar, M. J. S.; Zoebisch, E. G.; Healy, E. F.; Stewart, J. J. P. Development and use of quantum mechanical molecular models. 76. AM1: a new general purpose quantum mechanical molecular model. *J. Am. Chem. Soc.* **1985**, *107*, 3902−3909.

DOI: 10.1021/acs.jctc.6b00733
J. Chem. Theory Comput. 2017, 13, 191−201